IEEE Access
Multidisciplinary | Rapid Review | Open Access Journal

Received March 28, 2022, accepted April 11, 2022, date of publication April 18, 2022, date of current version April 22, 2022.

Digital Object Identifier 10.1109/ACCESS.2022.3168160

Accurate and Numerically Stable FDTD Modeling of Human Skin Tissues in THz Band

JAESUN PARK, JAE-WOO BAEK, AND KYUNG-YOUNG JUNG, (Senior Member, IEEE)
Department of Electronic Engineering, Hanyang University, Seoul 04763, South Korea

Corresponding author: Kyung-Young Jung (kyjung3@hanyang.ac.kr)

This work was supported by the National Research Foundation of Korea (NRF) Grant by the Korean Government through MSIT under Grant 2020R1F1A1055444.

ABSTRACT We propose finite-difference time-domain (FDTD) modeling suitable for healthy skin, basal cell carcinoma, dysplastic pigmentary nevus, and non-dysplastic pigmentary nevus in the frequency range of 0.25 THz to 1.05 THz. Toward this purpose, we utilize the complex-conjugate pole-residue (CCPR) dispersion model, because it is very simple to extract the accurate CCPR coefficients using the powerful vector fitting tool. In the FDTD method, it is of great importance to check the numerical stability conditions. If the coefficients extracted through the vector fitting tool do not satisfy the numerical stability conditions, the particle swarm optimization (PSO) algorithm is employed to obtain the accurate and numerically stable coefficients. Numerical examples are provided to validate our proposed FDTD modeling.

INDEX TERMS Dispersion model, dispersive media, finite-difference time-domain (FDTD) method, human skin tissues, terahertz (THz).

I. INTRODUCTION

In the case of basal cell carcinoma, which accounts for 75% of all skin cancers, the incidence in Europe is increasing by 5.5% per year in recent years [1], [2]. In addition, malignant melanoma, which evolves from dysplastic pigmentary nevus, accounts for 3% of skin cancers, and has gradually increased since the 1960s, with nearly 96,000 new cases in 2019 [3]. Early detection of these skin cancers is important because they have high metastasis and poor prognosis. Terahertz (THz) imaging technology for diagnosing skin cancer has been actively studied. Note that THz radiation is non-hazardous since it is non-ionizing and low average power for THz imaging is usually used [4]. THz imaging technology of skin cancer can differentiate healthy skin tissues and diseased skin tissues [5], [6]. For example, a THz pulsed system was used to image basal cell carcinoma *ex vivo* for total 21 samples [7]. When basal cell carcinoma and normal tissues are compared, basal cell carcinoma has much higher absorption at THz. Therefore, the regions of basal cell carcinoma marked by THz pulsed imaging systems have a high correlation with histology. In addition, THz radiation can be harnessed for cancer treatment because of its interaction with cellular components [8], [9]. Numerical methods are highly required to accurately analyze electromagnetic wave interaction with various human tissues in THz band.

Among many methods in computational electromagnetics [10]–[15], the finite-difference time-domain (FDTD) method has been widely used to analyze various electromagnetic wave problems due to its simplicity, robustness, and accuracy [16]–[26]. In addition, a wideband response can be obtained with a single time domain analysis. The FDTD method has been successfully used to analyze complex dispersive medium. Various dispersion models such as Debye, Drude, Lorentz, complex-conjugate pole-residue (CCPR), quadratic complex rational function (QCRF), and modified Lorentz (mLor) [27]–[38] have been introduced so far to examine electromagnetic wave interaction with dispersive media. The Debye dispersion model has been widely used for the dispersion modeling of human tissues and it was successfully used for healthy skin and basal cell carcinoma tissues in THz band [39]–[41]. In this work, the CCPR dispersion model is employed because it is a more general dispersion model of the Debye, Lorentz, and Drude models. Note that the Debye model requires one term per one pole, where both pole and residue must be real-valued and the CCPR model requires two terms (conjugate pairs) per one pole. However, the CCPR model has a higher degree of freedom than the Debye model because both pole and residue can have nonzero real and imaginary parts simultaneously, which indicating that fewer

The associate editor coordinating the review of this manuscript and approving it for publication was Lei Zhao.

poles are required for the CCPR model than the Debye model to have the same modeling accuracy. In addition, the sum of CCPR two terms cancels out the imaginary parts due to the complex conjugate property and thus FDTD computational operation can be reduced. Therefore, the computational efficiency of CCPR-based FDTD simulations is significantly enhanced than Debye-based FDTD simulations owing to the higher degree of freedom and complex-conjugate property [33], [36]–[38]. In addition, the CCPR parameters of dispersive media can be simply obtained by the powerful vector fitting tool [42]. Based on the CCPR dispersion model, we present an accurate FDTD modeling of four different types of human skin tissues such as healthy skin [39]–[41], [43], [44], basal cell carcinoma [39]–[41], [44], dysplastic pigmentary nevus [43], [44], and non-dysplastic pigmentary nevus [43], [44] in the THz range of 0.25 THz to 1.05 THz.

Due to the explicit solution of the time-dependent Maxwell curl equations, the FDTD simulation is conditionally stable [45], [46]. Therefore, it is very important to investigate the numerical stability conditions of dispersive FDTD modeling developed in this work. It must be checked whether the extracted CCPR coefficients satisfy the numerical stability conditions of the CCPR-FDTD formulation [47]. When the extracted CCPR parameters are not numerically stable, we employ the particle swarm optimization (PSO) algorithm [48], [49] to derive the CCPR parameters that satisfy the numerical stability conditions. This additional procedure can guarantee accurate and numerically stable FDTD modeling of human skin tissues. Numerical examples are employed to validate our proposed FDTD modeling for the four human skin tissues in the frequency of interest.

II. METHODOLOGY

Assuming an $e^{j\omega t}$ time dependence, the relative permittivity of the CCPR dispersion model [33] can be expressed as

$$\varepsilon_r(\omega) = \varepsilon_{r,\infty} + \sum_{q=1}^{M} \left(\frac{r_q}{j\omega - p_q} + \frac{r_q^*}{j\omega - p_q^*} \right) \tag{1}$$

where $\varepsilon_{r,\infty}$ is the relative permittivity at the infinite frequency, p_q (rad/s) and r_q (rad/s) denote the pole and residue of the CCPR model, respectively, M is the total number of the CCPR pairs, and * means the complex conjugate.

As alluded previously, the aim of this work is to develop accurate and stable FDTD dispersion modeling to perform electromagnetic wave analysis on various human skin tissues. First, FDTD dispersion modeling is based on the measurement data. When the measurement data are expressed as refractive index $n(\omega)$ and absorption coefficient $\alpha(\omega)$, they should be converted to the real part and the imaginary part of the relative permittivity using the following relations:

$$\varepsilon_r'(\omega) = n^2(\omega) - K^2(\omega) \tag{2}$$

$$\varepsilon_r''(\omega) = 2n(\omega)K(\omega) \tag{3}$$

where K is the extinction coefficient, defined as [50]

$$K(\omega) = \frac{\alpha(\omega)c_0}{2\omega} \tag{4}$$

and c_0 is the speed of light in free space, $c_0 = 1/\sqrt{\mu_0\varepsilon_0}$.

Next, the CCPR coefficients are extracted using the simple and powerful vector fitting tool [42]. The vector fitting tool can robustly provide rational function approximations for the measured values in the frequency domain because it does not fail for poorly selected initial guess. In addition, it is very easy to implement in a computer program with the aid of standard software packages which are used to solve matrix problems.

Note that even if the dynamic stability condition is satisfied, the numerical stability conditions may not be satisfied, since the discretization in both space and time domains is not considered in the dynamic stability condition [45], [51]. The dynamic stability condition for the CCPR dispersion model is $\mathrm{Re}(p) \le 0$, which can lead to stable and causal $\varepsilon_r(\omega)$ [33]. After utilizing this vector fitting tool, in this work, we check whether the derived CCPR parameters satisfy the numerical stability conditions [47]:

$$\mathrm{Re}(p) \le 0, \mathrm{Re}(r) \ge 0, Q \ge 0, \nu^2 \le 1 \tag{5}$$

where

$$Q = 2\mathrm{Re}(p)\mathrm{Re}(rp^*) - |p|^2\mathrm{Re}(r)$$

$$\nu^2 = (c_0\Delta t)^2 \sum_{\alpha=x,y,z} \frac{\sin^2(\widetilde{k}_\alpha \Delta_\alpha/2)}{(\Delta_\alpha)^2}.$$

In above, Δt is the FDTD time step size, Δ_α is the FDTD space step size, and $\widetilde{k}_\alpha$ denotes the numerical wavenumber in the α direction [47]. In the numerical stability analysis, $\sin^2(\widetilde{k}_\alpha \Delta_\alpha/2)$ is set as one for all possible numerical wavenumbers. Note that the above four numerical stability conditions are derived by the von Neumann method with the Routh-Hurwitz (R-H) criterion [27] and details can be found in [47]. The first numerical stability condition can be inferred from the dynamic stability condition and the last numerical stability condition is exactly same as the standard Courant–Friedrichs–Lewy (CFL) condition [52], [53].

In this work, if the CCPR parameters do not satisfy the above numerical stability conditions, the PSO algorithm [48], [49] is performed to extract the numerically stable coefficients. The PSO algorithm is one of the most popular optimization algorithms, which was developed with ideas from social behavior patterns of bee, bird, and fish groups. The PSO algorithm uses groups of particles called swarms and these particles navigate through the search space. Because each particle knows where it has moved before, it remembers the location with the most optimal fitness (pBest) among the positions it has passed, and shares the position with the best fitness in the swarm (gBest). By repeating this procedure, an optimal solution with the best fitness can be derived. In the PSO algorithm, the next position of each particle can be found from the following equation [49]:

$$v_n^{i+1} = v_n^i + c_1 \cdot \mathrm{rand}() \cdot (p\mathrm{Best}_n^i - x_n^i)$$

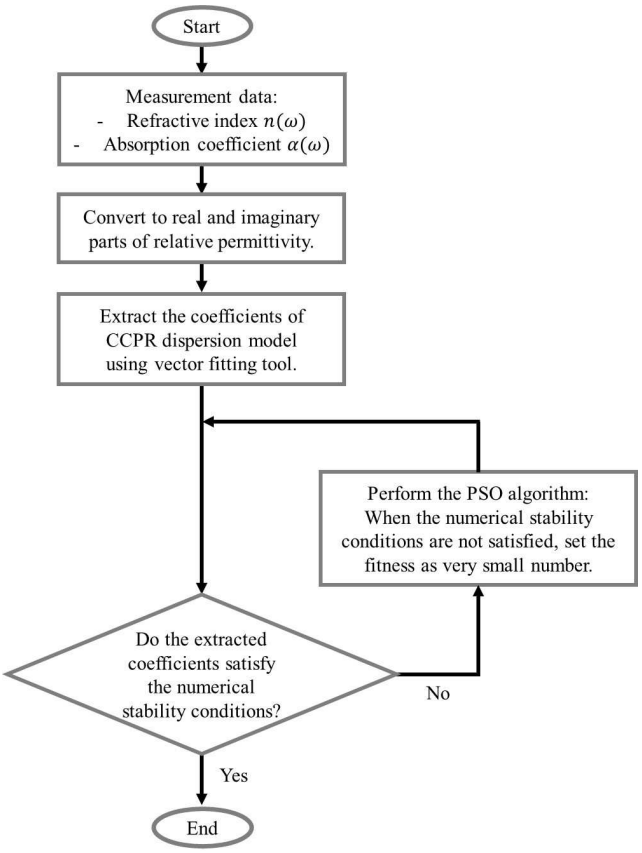

FIGURE 1. Flow chart for the proposed CCPR-FDTD dispersion modeling.

$$+c_2 \cdot \text{rand}() \cdot (g\text{Best}_n^i - x_n^i) \tag{6}$$

$$x_n^{i+1} = x_n^i + v_n^{i+1} \tag{7}$$

where v_n^{i+1} is the velocity of particle n at iteration $i+1$, x_n^i is the current position of particle n at iteration i, and rand() is a random number between 0 and 1. Also, c_1 is the cognitive parameter and represents confidence of particle in itself, and c_2 is the social parameter and denotes confidence of particle in its neighbors. These two parameters control the overall velocity of particle. When the value of the velocity is too large, particle may pass the position of the optimal solution, and when the velocity is too small, it may not be able to sufficiently explore the solution space. Therefore, the selection of the appropriate values of c_1 and c_2 is required. In this work, the fitness is defined as the inverse of root mean square relative error (RMSRE):

$$RMSRE = \sqrt{\frac{1}{N}\sum_{n=1}^{N}\left|\frac{\widetilde{\varepsilon_r}(\omega_n) - \varepsilon_r(\omega_n)}{\varepsilon_r(\omega_n)}\right|^2} \tag{8}$$

where N means the number of sampling frequencies, and $\widetilde{\varepsilon_r}$ and ε_r indicate the curve-fitted data and the measurement data, respectively. In the conventional PSO algorithm, an optimal solution is derived such that it leads to the best fitness.

TABLE 1. Numerically stable parameters of the CCPR dispersion model for healthy skin and basal cell carcinoma.

Tissue	Healthy skin	Basal cell carcinoma
$\varepsilon_{r,\infty}$	2.4637	2.7053
p_1	-4.274086e+11 +j4.525954e+11	-2.655093e+11 +j4.511042e+11
r_1	3.033024e+12 -j3.004377e+11	2.938155e+12 -j1.840979e+12
p_2		-1.701289e+11 +j7.493352e+12
r_2		2.547043e+10 -j5.976689e+11

In this work, an additional process is performed to extract the CCPR coefficients that satisfy the numerical stability conditions. In specific, when the CCPR coefficients are numerically unstable, we intentionally set the fitness value as a very small number so that the particles of the PSO algorithm can escape from the numerically unstable CCPR coefficients and find the new optimal CCPR coefficients that satisfy the numerical stability conditions. Fig. 1 shows the flow chart for CCPR-FDTD dispersion modeling developed in this work.

III. NUMERICAL EXAMPLES

As mentioned previously, we consider healthy skin, basal cell carcinoma, dysplastic pigmentary nevus, and non-dysplastic pigmentary nevus. The measurement data for refractive index $n(\omega)$ and absorption coefficient $\alpha(\omega)$ in the frequency range of 0.25 THz to 1.05 THz can be found in [44].

A. HEALTHY SKIN AND BASAL CELL CARCINOMA

First, we extract the parameters of the CCPR dispersion model for healthy skin and basal cell carcinoma by utilizing the powerful vector fitting technique only, as the conventional approach. Let us address the total CCPR pairs number (M). As the number of poles increases, the computational efficiency of the FDTD simulation decreases. In this work, the number of CCPR terms is determined when its RMSRE is equal to or less than 3% while gradually increasing the number of CCPR terms. The resulting CCPR parameters are listed in Table 1. It is confirmed that these extracted CCPR coefficients satisfy the numerical stability conditions of (5) as long as the FDTD time step size is limited by the CFL condition. Fig. 2 shows the complex relative permittivity of the CCPR dispersion model (solid red line) and measurement data (black dots) for healthy skin tissues. It is found out that the maximum error between the measured data and the fitted data is 4.7% and the RMSRE over the whole range of interest frequencies is 1.81%. The measured data and fitted data for basal cell carcinoma tissues are shown in Fig. 3 and its maximum error and the RMSRE are 2.5% and 1.3%, respectively. The numerically stable coefficients of the CCPR model can

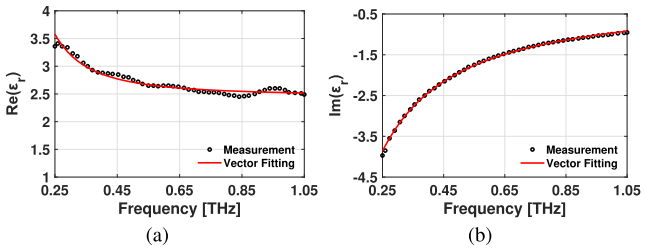

FIGURE 2. Complex relative permittivity of healthy skin. (a) Real part. (b) Imaginary part.

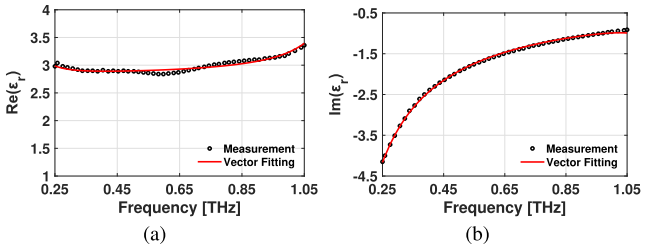

FIGURE 3. Complex relative permittivity of basal cell carcinoma. (a) Real part. (b) Imaginary part.

be accurately derived by employing only the powerful vector fitting tool for healthy skin and basal cell carcinoma.

B. DYSPLASTIC PIGMENTARY NEVUS AND NON-DYSPLASTIC PIGMENTARY NEVUS

For dysplastic pigmentary nevus and non-dysplastic pigmentary nevus, it is found out that the CCPR parameters that satisfy the numerical stability conditions of (5) cannot be obtained by using the vector fitting tool only, different from the previous two skin tissues. To illustrate this, we first extract CCPR dispersion modeling of dysplastic pigmentary nevus by utilizing only the vector fitting tool. The resulting CCPR parameters are listed in Table 2. Fig. 4 shows that the CCPR parameters agree well with the measurement data and its RMSRE is 1.78%. Albeit with good accuracy, this CCPR dispersion modeling cannot be employed for the electromagnetic analysis of dysplastic pigmentary nevus due to numerical instability, which will be shown later.

Next, the CCPR parameters are extracted by using the vector fitting tool and the PSO algorithm simultaneously. In this work, we set the maximum number of iteration as 30, and the swarm size as 8000 for the PSO algorithm. Also, the number of independent trials is set to 30, and since the best RMSRE is derived when the cognitive parameter c_1 and the social parameter c_2 are 2, respectively, these values are used in this work. As mentioned previously, when the CCPR coefficients do not satisfy the numerical stability conditions, we deliberately set the fitness as a very small value. Table 3 shows the CCPR parameters for dysplastic pigmentary nevus and non-dysplastic pigmentary nevus by employing our proposed technique. Fig. 5 shows the measurement data (black dots) and the complex permittivity fitted through the CCPR dispersion model (red solid line) for dysplastic pigmentary

TABLE 2. Numerically unstable CCPR parameters for dysplastic pigmentary nevus using the vector fitting tool only.

Tissue	Dysplastic pigmentary nevus		
$\varepsilon_{r,\infty}$	1.6372		
p_1	-2.087355e+10 +j4.700033e+11	p_3	-3.001965e+11 +j6.973276e+12
r_1	2.336508e+12 -j4.973898e+11	r_3	-3.958382e+11 +j5.805459e+11
p_2	-1.233171e+12 +j2.096506e+12	p_4	-5.954187e+11 +j8.440071e+12
r_2	3.387774e+11 -j5.810715e+11	r_4	1.311179e+12 -j4.861221e+12

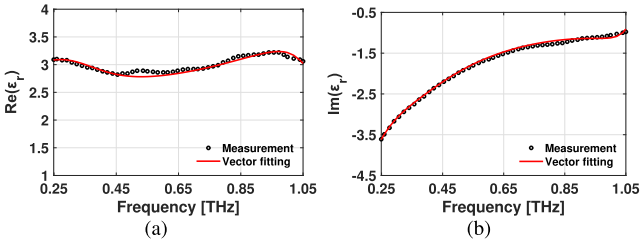

FIGURE 4. Complex relative permittivity of dysplastic pigmentary nevus fitted through only the vector fitting tool. (a) Real part. (b) Imaginary part.

nevus. The maximum error of the fitted data against the measured data for dysplastic pigmentary nevus is 4.9% and the RMSRE over the whole frequencies is 2.05%. The plot of the measurement data of non-dysplastic pigmentary nevus and its fitted complex permittivity is shown in Fig. 6. It is observed that its maximum error and the RMSRE are 4.13% and 2.17%, respectively.

Now, we perform actual FDTD simulations to investigate numerical stability of CCPR-FDTD modelings. For simplicity (without loss of generality), one-dimensional (1-D) electromagnetic analysis for dysplastic pigmentary nevus is considered as shown in Fig. 7. In the FDTD simulations, the time step size $\Delta t = C_n \Delta z / c_0$ and the Courant number $C_n = 0.99$ [52], [53] are employed and the FDTD grid size of $\Delta z = 1.1 \mu m$ is used. Note that the FDTD grid size is chosen such that the point per wavelength (PPW) is larger than 100 for the smallest wavelength in the frequency range of interest. The whole computational domain consists of 2000 FDTD cells with 1000 FDTD cells of the free space and the other 1000 FDTD cells of dysplastic pigmentary nevus. The sinewave-modulated Gaussian pulse with x-polarization is excited in the free space and denoted as

$$M_x(t) = \sin(2\pi f_0 t) e^{-\frac{(t-t_0)^2}{t_w^2}} \tag{9}$$

where f_0 is the center frequency, t_0 is the time delay, and t_w is the half width of the pulse. In this work, $f_0 = 0.65$ THz, $t_0 = 4.43$ ps, and $t_w = 1.48$ ps to consider the frequency range of interest. Also, the 10 layers of perfectly matched layer (PML) are used for the absorbing boundary condition [16]. Fig. 8(a)

TABLE 3. Numerically stable parameters of the CCPR dispersion model for dysplastic pigmentary nevus and non-dysplastic pigmentary nevus extracted using the vector fitting tool and the PSO algorithm simultaneously.

Tissue	Dysplastic pigmentary nevus	Non-dysplastic pigmentary nevus
$\varepsilon_{r,\infty}$	2.3860	3.0999
p_1	-6.528833e+10 +j4.150680e+10	-1.570256e+09 -j7.119344e+10
r_1	1.888419e+12 -j2.634479e+13	4.117588e+10 +j5.599484e+13
p_2	-1.579397e+12 -j1.538612e+12	-7.693030e+11 +j9.004962e+11
r_2	4.564776e+11 +j1.851527e+12	3.129868e+12 -j1.184645e+12
p_3	-1.986944e+12 -j9.122916e+12	
r_3	3.129761e+11 +j1.300466e+12	
p_4	-6.66427e+12 -j1.291568e+13	
r_4	1.346255e+12 +j2.669277e+12	

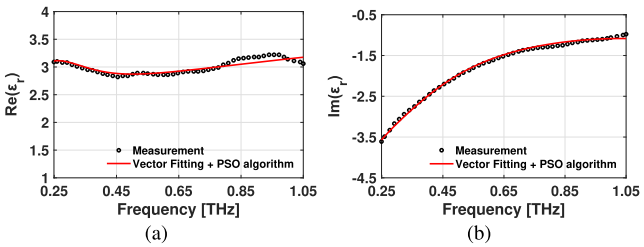

FIGURE 5. Complex relative permittivity of dysplastic pigmentary nevus fitted through the vector fitting tool and the PSO algorithm simultaneously. (a) Real part of complex permittivity. (b) Imaginary part of complex permittivity.

shows E_x at the discontinuity interface when the numerically unstable CCPR parameters (Table 2) are used. As expected from our previous observation, the FDTD simulation suffers from numerical instability, although the CCPR parameters are in good agreement with the measurement data. Fig. 8(b) shows the E_x counterpart for the numerically stable CCPR parameters (Table 3) are used. Numerical stability is observed since the CCPR parameters satisfy the numerical stability conditions of (5).

Next, we investigate the reflection coefficient for numerically stable CCPR-FDTD simulations for four different human skin tissues. FDTD simulation results for four human skin tissues and the theoretical results [44] are in good agreement with each other. The RMSRE for the reflection coefficients of the four types of skin tissues is 2.21% (healthy skin), 1.73% (basal cell carcinoma), 2.1% (dysplastic pigmentary nevus), and 1.68% (non-dysplastic pigmentary nevus). The amplitude and phase of the reflection coefficients change with the frequency. The amplitude of the

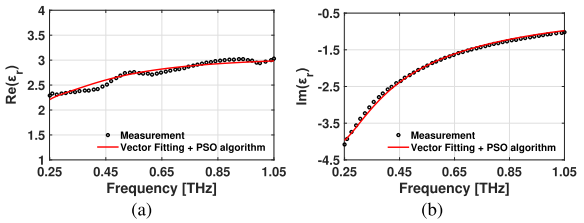

FIGURE 6. Complex relative permittivity of non-dysplastic pigmentary nevus fitted through the vector fitting tool and the PSO algorithm simultaneously. (a) Real part of complex permittivity. (b) Imaginary part of complex permittivity.

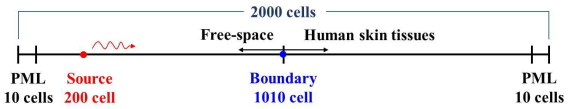

FIGURE 7. FDTD simulation setup.

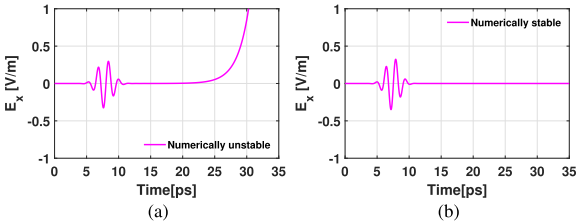

FIGURE 8. 1-D FDTD simulation results for dysplastic pigmentary nevus. (a) Unstable CCPR-FDTD. (b) Stable CCPR-FDTD.

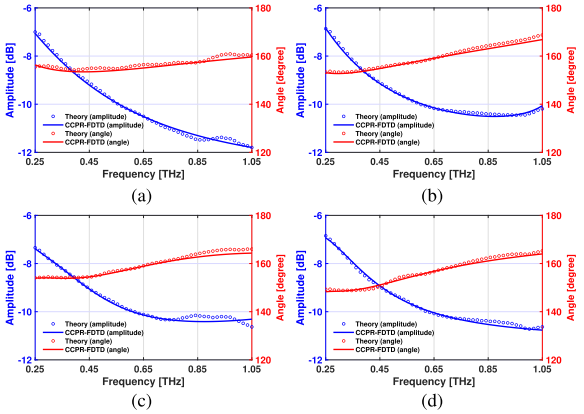

FIGURE 9. Reflection coefficient for four human skin tissues. (a) Healthy skin. (b) Basal cell carcinoma (c) Dysplastic pigmentary nevus (d) Non-dysplastic pigmentary nevus.

reflection coefficient is inversely proportional to the frequency in 0.25 THz - 0.75 THz and the phase of the reflection coefficient is generally proportional to the frequency. The electromagnetic response depends on the skin tissue type. It is clearly observed that the amplitude slope (versus the frequency) of healthy skin tissue is the steepest and its phase slope (versus the frequency) is the flattest among four human tissues. Our proposed FDTD dispersion modeling of human skin tissues can be used to understand electromagnetic phenomena of human skin tissues and provide in-depth foundation for systematic development of THz imaging technology as well as THz therapeutics. For example, the optimal system parameters such as the operating frequency and the

bandwidth can be found by various numerical simulations based on our FDTD modeling. In addition, our work can be useful for studying THz tumor diagnosis methodology such as the Cole-Cole diagram [43], [44] and its principal component analysis [43].

IV. CONCLUDING REMARKS

In the previous works [39]–[41], FDTD dispersion modeling was presented for healthy skin and basal cell carcinoma tissues but there is no literature for dysplastic pigmentary nevus and non-dysplastic pigmentary nevus. In this work, we have proposed accurate and robust FDTD modeling for healthy skin, basal cell carcinoma, dysplastic pigmentary nevus, and non-dysplastic pigmentary nevus. For accurate FDTD modeling of various human skin tissues, we employ the CCPR dispersion model since accurate CCPR parameters can be simply extracted by utilizing the vector fitting tool. First, the coefficients of the CCPR dispersion model for four different skin tissues are extracted using the vector fitting tool. Then, it is checked whether the extracted coefficients satisfy the numerical stability conditions or not. If the parameters are not numerically stable, the PSO algorithm is employed to obtain the numerically stable and accurate CCPR coefficients. It should be noted that, in this work, the numerical stability conditions are merged into the PSO algorithm so that the extracted CCPR coefficients can lead to numerical stable FDTD analysis. For healthy skin and basal cell carcinoma, the vector fitting tool is enough to extract the numerically stable CCPR coefficients and the RMSREs are less than 2%. On the other hand, the vector fitting tool and the PSO algorithm should be employed simultaneously for dysplastic pigmentary nevus and non-dysplastic pigmentary nevus to obtain accurate and robust FDTD dispersion modeling. It is observed that the RMSRE for dysplastic pigmentary nevus is 2.05% and the RMSRE for non-dysplastic pigmentary nevus is 2.17%. Actual FDTD simulations are performed to validate CCPR-FDTD modeling developed in this work. Although our accurate and robust FDTD dispersion model is applied for the CCPR dispersion model of various human skin tissues, it can be easily extended to other dispersion model of general complex dispersive media in a similar fashion. In the future, more practical 3-D examples for skin cancers will be conducted, similar to breast cancer examples [26].

REFERENCES

[1] S. C. Flohil, I. Seubring, M. M. van Rossum, J.-W.-W. Coebergh, E. de Vries, and T. Nijsten, "Trends in basal cell carcinoma incidence rates: A 37-year Dutch observational study," *J. Investigative Dermatol.*, vol. 133, no. 4, pp. 913–918, Apr. 2013.

[2] M. Seidl-Philipp, N. Frischhut, N. Höllweger, M. Schmuth, and V. A. Nguyen, "Known and new facts on basal cell carcinoma," *J. der Deutschen Dermatologischen Gesellschaft*, vol. 19, no. 7, pp. 1021–1041, Jul. 2021.

[3] P. P. Naik, "Cutaneous malignant melanoma: A review of early diagnosis and management," *World J. Oncol.*, vol. 12, no. 1, pp. 7–19, Feb. 2021.

[4] R. M. Woodward, B. E. Cole, V. P. Wallace, R. J. Pye, D. D. Arnone, E. H. Linfield, and M. Pepper, "Terahertz pulse imaging in reflection geometry of human skin cancer and skin tissue," *Phys. Med. Biol.*, vol. 47, no. 21, pp. 3853–3863, Oct. 2002.

[5] V. P. Wallace, A. J. Fitzgerald, E. Pickwell, R. J. Pye, P. F. Taday, N. Flanagan, and T. Ha, "Terahertz pulsed spectroscopy of human basal cell carcinoma," *Appl. Spectrosc.*, vol. 60, no. 10, pp. 1127–1133, Oct. 2006.

[6] V. P. Wallace, A. J. Fitzgerald, S. Shankar, N. Flanagan, R. Pye, J. Cluff, and D. D. Arnone, "Terahertz pulsed imaging of basal cell carcinoma *ex vivo* and *in vivo*," *Brit. J. Dermatol.*, vol. 151, no. 2, pp. 424–432, Aug. 2004.

[7] R. M. Woodward, V. P. Wallace, R. J. Pye, B. E. Cole, D. D. Arnone, E. H. Linfield, and M. Pepper, "Terahertz pulse imaging of *ex vivo* basal cell carcinoma," *J. Investigative Dermatol.*, vol. 120, no. 1, pp. 72–78, Jan. 2003.

[8] M.-O. Mattsson, O. Zeni, and M. Simkó, "Is there a biological basis for therapeutic applications of millimetre waves and THz waves?" *J. Infr., Millim., THz Waves*, vol. 39, no. 9, pp. 863–878, Mar. 2018.

[9] M. Simko and M.-O. Mattsson, "Terahertz electromagnetic fields in diagnostic and therapeutic settings–potentials and challenges," in *Pulsed Electromagnetic Fields for Clinical Applications*. Boca Raton, FL, USA: CRC Press, 2020, ch. 14.

[10] S. Mikki, A. M. Alzahed, and Y. M. M. Antar, "The spatial singularity expansion method for electromagnetics," *IEEE Access*, vol. 7, pp. 124576–124595, 2019.

[11] M. Ayari, Y. E. Touati, and S. Altowaijri, "Method of moments versus advanced transverse wave approach for EM validation of complex microwave and RF applications," *J. Electromagn. Eng. Sci.*, vol. 20, no. 1, pp. 31–38, Jan. 2020.

[12] M. Bozorgi, "A mode-matching solution for TE-backscattering from an arbitrary 2D rectangular groove in a PEC," *J. Electromagn. Eng. Sci.*, vol. 20, no. 3, pp. 159–163, Jul. 2020.

[13] V. Srinivasan, M. Fernando, S. Kumara, T. Selvaraj, and V. Cooray, "Modeling and assessment of lightning hazards to humans in heritage monuments in India and Sri Lanka," *IEEE Access*, vol. 8, pp. 228032–228048, 2020.

[14] K.-C. Kim, G.-S. Park, G.-J. Min, and Y.-K. Cho, "Resonance transmission of dual plates with narrow small slots due to two parallel wires for frequencies around 2 GHz," *J. Electromagn. Eng. Sci.*, vol. 21, no. 4, pp. 253–260, Sep. 2021.

[15] D.-Y. Lee, J.-I. Lee, and D.-W. Seo, "Dynamic RCS estimation according to drone movement using the MoM and far-field approximation," *J. Electromagn. Eng. Sci.*, vol. 21, no. 4, pp. 322–328, Sep. 2021.

[16] A. Taflove and S. C. Hagness, *Computational Electrodynamics: The Finite-Difference Time-Domain method*, 3rd ed. Norwood, MA, USA: Artech House, 2005.

[17] R. A. Chilton, K. Y. Jung, R. Lee, and F. L. Teixeira, "Frozen modes in parallel-plate waveguides loaded with magnetic photonic crystals," *IEEE Trans. Microw. Theory Techn.*, vol. 55, no. 12, pp. 2631–2641, Dec. 2007.

[18] S. D. Gedney, *Introduction to Finite-Difference Time-Domain (FDTD) Method for Electromagnetics*. Lexington, KY, USA: Morgan & Claypool, 2010.

[19] J.-W. Baek, D.-K. Kim, and K.-Y. Jung, "Finite-difference time-domain modeling for electromagnetic wave analysis of human voxel model at millimeter-wave frequencies," *IEEE Access*, vol. 7, pp. 3635–3643, 2019.

[20] J. Cho, M.-S. Park, and K.-Y. Jung, "Perfectly matched layer for accurate FDTD for anisotropic magnetized plasma," *J. Electromagn. Eng. Sci.*, vol. 20, no. 4, pp. 277–284, Oct. 2020.

[21] S.-Y. Hyun, "Improved discrete-time boundary condition for the thin-wire FDTD analysis of lossy insulated cylindrical antennas located in lossy media," *J. Electromagn. Eng. Sci.*, vol. 21, no. 1, pp. 60–63, Jan. 2021.

[22] Y.-J. Kim and K.-Y. Jung, "Accurate and efficient finite-difference time-domain formulation of dusty plasma," *IEEE Trans. Antennas Propag.*, vol. 69, no. 10, pp. 6600–6606, Oct. 2021.

[23] S. Jang and K.-Y. Jung, "Perfectly matched layer formulation of the INBC-FDTD algorithm for electromagnetic analysis of thin film materials," *IEEE Access*, vol. 9, pp. 118099–118106, 2021.

[24] K. Niu, Z. Huang, B. Wu, and X. Wu, "3D optimised hybrid implicit–explicit FDTD method with suppressed numerical dispersion," *Electron. Lett.*, vol. 54, no. 6, pp. 335–336, Mar. 2018.

[25] G. Xie, Z. Huang, M. Fang, and W. E. I. Sha, "Simulating Maxwell–Schrödinger equations by high-order symplectic FDTD algorithm," *IEEE J. Multiscale Multiphys. Comput. Techn.*, vol. 4, pp. 143–151, 2019.

[26] A. F. Mirza, F. Abdulsalam, R. Asif, Y. A. S. Dama, M. M. Abusitta, F. Elmegri, R. A. Abd-Alhameed, J. M. Noras, and R. Qahwaji, "Breast cancer detection using 1D, 2D, and 3D FDTD numerical methods," in *Proc. IEEE Int. Conf. Comput. Inf. Technol., Ubiquitous Comput. Commun., Dependable, Autonomic Secure Comput., Pervasive Intell. Comput.*, Oct. 2015, pp. 1042–1045.

[27] A. Pereda, L. A. Vielva, A. Vegas, and A. Prieto, "Analyzing the stability of the FDTD technique by combining the von Neumann method with the Routh-Hurwitz criterion," *IEEE Trans. Microw. Theory Techn.*, vol. 49, no. 2, pp. 377–381, Feb. 2001.
[28] K.-Y. Jung, F. L. Teixeira, and R. M. Reano, "Au/SiO_2 nanoring plasmon waveguides at optical communication band," *J. Lightw. Technol.*, vol. 25, no. 9, pp. 2757–2765, Sep. 2007.
[29] A. Deinega and S. John, "Effective optical response of silicon to sunlight in the finite-difference time-domain method," *Opt. Lett.*, vol. 37, no. 1, pp. 112–114, Jan. 2012.
[30] K. P. Prokopidis and D. C. Zografopoulos, "A unified FDTD/PML scheme based on critical points for accurate studies of plasmonic structures," *J. Lightw. Technol.*, vol. 31, no. 15, pp. 2467–2476, Aug. 1, 2013.
[31] S.-G. Ha, J. Cho, J. Choi, H. Kim, and K.-Y. Jung, "FDTD dispersive modeling of human tissues based on quadratic complex rational function," *IEEE Trans. Antennas Propag.*, vol. 61, no. 2, pp. 996–999, Feb. 2013.
[32] H. Choi, J.-W. Baek, and K.-Y. Jung, "Comprehensive study on numerical aspects of modified Lorentz model-based dispersive FDTD formulations," *IEEE Trans. Antennas Propag.*, vol. 67, no. 12, pp. 7643–7648, Dec. 2019.
[33] M. Han, R. W. Duttonm, and S. Fan, "Model dispersive media in finite-difference time-domain method with complex-conjugate pole-residue pairs," *IEEE Microw. Wireless Compon. Lett.*, vol. 16, no. 3, pp. 119–121, Mar. 2006.
[34] H. Choi, Y.-H. Kim, J.-W. Baek, and K.-Y. Jung, "Accurate and efficient finite-difference time-domain simulation compared with CCPR model for complex dispersive media," *IEEE Access*, vol. 7, pp. 160498–160505, 2019.
[35] Y.-H. Kim, H. Choi, J. Cho, and K.-Y. Jung, "FDTD modeling for the accurate electromagnetic wave analysis of graphene," *J. Electr. Eng. Technol.*, vol. 15, no. 3, pp. 1281–1286, May 2020.
[36] H. Lin, M. F. Pantoja, L. D. Angulo, J. Alvarez, R. G. Martin, and S. G. Garcia, "FDTD modeling of graphene devices using complex conjugate dispersion material model," *IEEE Microw. Wireless Compon. Lett.*, vol. 22, no. 12, pp. 612–614, Dec. 2012.
[37] I. Udagedara, M. Premaratne, U. D. Rukhlenko, H. T. Hattori, and G. P. Agrawal, "Unified perfectly matched layer for finite-difference time-domain modeling of dispersive optical materials," *Opt. Exp.*, vol. 17, no. 23, pp. 21179–21190, Nov. 2009.
[38] M. Han, Z. Yu, and S. Fan, "Efficient treatment of dispersive electric permittivity in finite-difference time-domain simulations of advanced photonic devices," in *Proc. Numer. Simulation Optoelectronic Devices*, Sep. 2010, pp. 113–114.
[39] E. Pickwell, A. J. Fitzgerald, B. E. Cole, P. F. Taday, R. J. Pye, T. Ha, M. Pepper, and V. P. Wallace, "Simulating the response of terahertz radiation to basal cell carcinoma using *ex vivo* spectroscopy measurements," *J. Biomed. Opt.*, vol. 10, no. 6, 2005, Art. no. 064021.
[40] B. C. Q. Truong, H. Duong Tuan, H. H. Kha, and H. T. Nguyen, "Debye parameter extraction for characterizing interaction of terahertz radiation with human skin tissue," *IEEE Trans. Biomed. Eng.*, vol. 60, no. 6, pp. 1528–1537, Jun. 2013.
[41] B. C. Q. Truong, H. D. Tuan, V. P. Wallace, A. J. Fitzgerald, and H. T. Nguyen, "The potential of the double Debye parameters to discriminate between basal cell carcinoma and normal skin," *IEEE Trans. THz Sci. Technol.*, vol. 5, no. 6, pp. 990–998, Nov. 2015.
[42] B. Gustavsen and A. Semlyen, "Rational approximation of frequency domain responses by vector fitting," *IEEE Trans. Power Del.*, vol. 14, no. 3, pp. 1052–1061, Jul. 1999.
[43] K. I. Zaytsev, K. G. Kudrin, V. E. Karasik, I. V. Reshetov, and S. O. Yurchenko, "*In vivo* terahertz spectroscopy of pigmentary skin nevi: Pilot study of non-invasive early diagnosis of dysplasia," *Appl. Phys. Lett.*, vol. 106, no. 5, Feb. 2015, Art. no. 053702.
[44] K. I. Zaytsev, K. G. Kudrin, I. V. Reshetov, A. A. Gavdush, N. V. Chernomyrdin, V. E. Karasik, and S. O. Yurchenko, "*In vivo* spectroscopy of healthy skin and pathology in terahertz frequency range," *J. Phys., Conf. Ser.*, vol. 584, Jan. 2015, Art. no. 012023.
[45] J. Cho, S.-G. Ha, Y. B. Park, H. Kim, and K.-Y. Jung, "On the numerical stability of finite-difference time-domain for wave propagation in dispersive media using quadratic complex rational function," *Electromagnetics*, vol. 34, no. 8, pp. 625–632, Oct. 2014.
[46] J. Park and K.-Y. Jung, "Numerical stability of the modified Lorentz FDTD unified from various dispersion models," *Opt. Exp.*, vol. 29, no. 14, pp. 21639–21654, Jul. 2021.
[47] H. Choi, J.-W. Baek, and K.-Y. Jung, "Numerical stability and accuracy of CCPR-FDTD for dispersive medi," *IEEE Trans. Antennas Propag.*, vol. 68, no. 11, pp. 7717–7720, Nov. 2020.
[48] S. Mirjalili and S. Z. M. Hashim, "A new hybrid PSOGSA algorithm for function optimization," in *Proc. Int. Conf. Comput. Inf. Appl.*, Dec. 2010, pp. 374–377.
[49] D. Wang, D. Tan, and L. Liu, "Particle swarm optimization: An overview," *Soft Comput.*, vol. 22, pp. 387–408, Jan. 2018.
[50] K. Yang, A. Alomainy, and Y. Hao, "*In-vivo* characterisation and numerical analysis of the THz radio channel for nanoscale body-centric wireless networks," in *Proc. USNC-URSI Radio Sci. Meeting (AP-S Symp.)*, Lake Buena Vista, FL, USA, Jul. 2013, pp. 218–219.
[51] F. L. Teixeira and W. C. Chew, "On causality and dynamic stability of perfectly matched layers for FDTD simulations," *IEEE Trans. Microw. Theory Techn.*, vol. 47, no. 6, pp. 775–785, Jun. 1999.
[52] R. Courant, K. Friedrichs, and H. Lewy, "On the partial difference equations of mathematical physics," *IBM J. Res. Develop.*, vol. 11, no. 2, pp. 215–234, Mar. 1967.
[53] A. Fanti, M. Spanu, M. B. Lodi, F. Desogus, and G. Mazzarella, "Nonlinear analysis of soil microwave heating: Application to agricultural soils disinfection," *IEEE J. Multiscale Multiphys. Comput. Techn.*, vol. 2, pp. 105–114, 2017.
[54] C. A. Balanis, *Advanced Engineering Electromagnetics*. Hoboken, NJ, USA: Wiley, 1989.

JAESUN PARK received the B.S. degree in communication engineering from Daejin University, Pocheon, South Korea, in 2018. She is currently pursuing the M.S. degree with the Department of Electronic Engineering, Hanyang University, Seoul, South Korea. Her current research interests include computational electromagnetics and bio-electromagnetics.

JAE-WOO BAEK received the B.S. degree in electronics and information engineering from Korea University, Sejong, South Korea, in 2015, and the M.S. degree in electrical engineering from Hanyang University, Seoul, South Korea, in 2017, where he is currently pursuing the Ph.D. degree with the Department of Electronic Engineering. His current research interests include computational electromagnetics, bio-electromagnetics, and parallel programming.

KYUNG-YOUNG JUNG (Senior Member, IEEE) received the B.S. and M.S. degrees in electrical engineering from Hanyang University, Seoul, South Korea, in 1996 and 1998, respectively, and the Ph.D. degree in electrical and computer engineering from The Ohio State University, Columbus, OH, USA, in 2008.

From 2008 to 2009, he was a Postdoctoral Researcher with The Ohio State University. From 2009 to 2010, he was an Assistant Professor with the Department of Electrical and Computer Engineering, Ajou University, Suwon, South Korea. Since 2011, he has been with Hanyang University, where he is currently a Full Professor with the Department of Electronic Engineering. His current research interests include computational electromagnetics, bio-electromagnetics, and nano-electromagnetics.

Dr. Jung was a recipient of the Graduate Study Abroad Scholarship from the National Research Foundation of Korea, the Presidential Fellowship from The Ohio State University, the HYU Distinguished Teaching Professor Award from Hanyang University, and the Outstanding Research Award from the Korean Institute of Electromagnetic Engineering Society.